Biophysical Reports

REPORT

A comparative study of interfacial environments in lipid nanodiscs and vesicles

Xiao You,[1] Naveen Thakur,[2] Arka Prabha Ray,[2] Matthew T. Eddy,[2,*] and Carlos R. Baiz[1,*]
[1]Department of Chemistry, the University of Texas at Austin, Austin, Texas and [2]Department of Chemistry, University of Florida, Gainesville, Florida

ABSTRACT Membrane protein conformations and dynamics are driven by the protein-lipid interactions occurring within the local environment of the membrane. These environments remain challenging to accurately capture in structural and biophysical experiments using bilayers. Consequently, there is an increasing need for realistic cell-membrane mimetics for *in vitro* studies. Lipid nanodiscs provide certain advantages over vesicles for membrane protein studies. Nanodiscs are increasingly used for structural and spectroscopic characterization of membrane proteins. Despite the common use of nanodiscs, the interfacial environments of lipids confined to a ~10-nm diameter area have remained relatively underexplored. Here, we use ultrafast two-dimensional infrared spectroscopy and temperature-dependent infrared absorption measurements of the ester carbonyls to compare the interfacial hydrogen bond structure and dynamics in lipid nanodiscs of varying lipid compositions and sizes with ~100-nm vesicles. We examine the effects of lipid composition and nanodisc size. We found that nanodiscs and vesicles share largely similar lipid-water H-bond environments and interfacial dynamics. Differences in measured enthalpies of H-bonding suggest that H-bond dynamics in nanodiscs are modulated by the interaction between the annular lipids and the scaffold protein.

WHY IT MATTERS Mimetics of cellular membranes are widely employed in the biophysical and biochemical characterization of membrane proteins. A critical step in preparing samples for such studies is selecting suitable mimetics that preserve the structure and function of membrane proteins in environments that allow sample manipulation in aqueous solutions. Lipid nanodiscs are one of the most widely used cellular membrane mimetics, particularly in protein structural characterization. Thus, it is critical to understand the interfacial H-bond environment in nanodiscs to assess the impact on membrane proteins.

INTRODUCTION

Membrane proteins play a critical role in numerous cellular processes including signaling and transport (1). Membranes provide both a support structure for proteins and highly heterogeneous interfaces that regulate biochemical processes in the cell (2). The lipid composition and membrane environment influences the topologies, orientations, and, ultimately, the function of transmembrane and membrane-associated proteins (3–5). Thus, significant efforts have been directed at developing membrane mimetics for structural and functional studies of membrane proteins that mirror certain properties of native cell membranes. Specific protein-lipid interactions, such as electrostatics or hydrogen bonding (6–8), require the use of a suitable membrane-mimicking environment. Nanodiscs, composed of a phospholipid bilayer encircled by amphipathic membrane scaffold proteins (MSPs) (9,10), form soluble disc-shaped structures that serve as a detergent-free phospholipid vehicle for solution-phase studies of membrane proteins. Lipid nanodiscs are among the most popular cellular membrane mimetics and are used extensively for NMR spectroscopy (11–17), fluorescence spectroscopy (18–21), cryoelectron microscopy (22–25), and mass spectrometry (26–28), along with several other methods (29–32).

To date, research efforts have been focused on the properties of MSPs, the lipid compositions and shapes of nanodiscs, and their structural dynamics (33–39). However, the H-bond environment at the lipid-water interface in nanodiscs is not well understood. Previous studies have shown that the balance between lipid-lipid

Submitted May 10, 2022, and accepted for publication July 19, 2022.
*Correspondence: matthew.eddy@chem.ufl.edu or cbaiz@cm.utexas.edu
Editor: Erdinc Sezgin.
https://doi.org/10.1016/j.bpr.2022.100066

and lipid-water interactions modulates H-bond networks in vesicles and stacked multibilayers (40–44). Here, we characterize the interfacial environments in lipid nanodiscs and benchmark the measurements against lipid vesicles with the same phospholipid compositions. We measure H-bond populations, enthalpies, and local H-bond dynamics using a combination of temperature-dependent Fourier-transform infrared (FTIR) spectroscopy and ultrafast two-dimensional IR (2D IR) spectroscopy (45). Ester carbonyls are precisely located at the 1-nm boundary between the hydrophobic and hydrophilic regions of the interface and, as such, are unique vibrational reporters of the interfacial environment. We compare FTIR and 2D IR spectra of the ester carbonyl stretching mode in vesicles and nanodiscs of three different sizes from 8 to 12 nm in diameter (Fig. 1).

MATERIALS AND METHODS

Preparation of lipid vesicles

Lipid solutions, 1-palmitoyl-2-oleoyl-glycero-3-phosphocholine (POPC) at 25 mg/mL in chloroform, and 1-palmitoyl-2-oleoyl-sn-glycero-3-phospho-L-serine (POPS) at 10 mg/mL in chloroform were purchased from Avanti Polar Lipids (Birmingham, AL, USA), stored at −25°C, and used without further purification. Vesicles were prepared by evaporating the chloroform solvent by passing a dry nitrogen stream followed by desiccation under a mild vacuum. POPC, POPS, and a POPC:POPS mixture were then reconstituted in D_2O to 50 mg/mL for all solutions. Reconstituted samples were subject to six freeze-thaw cycles and 20-minute sonication, followed by extrusion through 100-nm-pore filters at 60°C to obtain uniform 100-nm vesicles (41). The lipid vesicle samples were stored at 4°C prior to FTIR and 2D IR measurements.

Expression and purification of MSP variants

MSP variants were expressed and purified according to published protocols (11,46). Additional details are provided in Section S1.

Assembly of MSP-lipid nanodiscs

Nanodiscs were assembled according to protocols reported in previous studies (11,18,46) that were adapted and further optimized. POPC and POPS lipids in powder form were solubilized in a buffer containing 25 mM Tris (pH 8.0), 150 mM NaCl, and 200 mM sodium cholate at 100 mM final lipid concentration and then mixed in desired molar ratios. Solutions containing lipids and purified MSPs were then mixed in molar ratios of 1:40 (MSP1D1ΔH5:lipids), 1:50 (MSP1D1:lipids), or 1:120 (MSP1E3D1:lipids). The resulting mixture was incubated for 4 hours at 4°C. Subsequently, bio-beads (Bio-Rad Laboratories) were added, and the reaction proceeded overnight at 4°C. Following overnight incubation, bio-beads were removed, and the samples were concentrated to the final concentrations for IR experiments using a Vivaspin 6 concentrator with a 30 kDa MWCO (Cytiva).

IR absorption spectroscopy

FTIR spectra were recorded on a Bruker Vertex 70 spectrometer. The spectrometer and sample chamber were purged with dry air to minimize absorptions from water vapor. Aqueous suspensions of vesicles or nanodiscs were held between two CaF_2 windows separated by a 25-μm PTFE spacer in a temperature-controlled sample cell. The sample cell was equilibrated for 5 min at each temperature setpoint using a recirculating chiller. Both sample and D_2O background spectra were measured at the following temperatures: 5°C, 10°C, 15°C, 20°C, 25°C, 30°C, 35°C, 40°C, 45°C, and 50°C.

Ultrafast 2D IR spectroscopy and data analysis

The 2D IR spectrometer has been described previously (47). 2D IR measurements in this study consist of excitation pulses (pump) and a detection pulse (probe) resonant with the carbonyl stretching mode in lipids. In brief, 100 fs mid-IR pulses were generated using an optical parametric amplifier and difference-frequency generation setup pumped by a Ti:Sapphire laser (Astrella, Coherent) and then split into the pump and probe pulses. The pump pulses were then generated by a pulse shaper (QuickShape, PhaseTech) and then spatially and temporarily overlapped with the probe pulse at the sample cell. The timing between the pump and probe was controlled by a delay stage. The 2D IR signal was measured using a spectrometer with an MCT array detector (Teledyne), which was used to resolve the probe frequency axis. The pump frequency axis was resolved through a numerical Fourier transformation of the

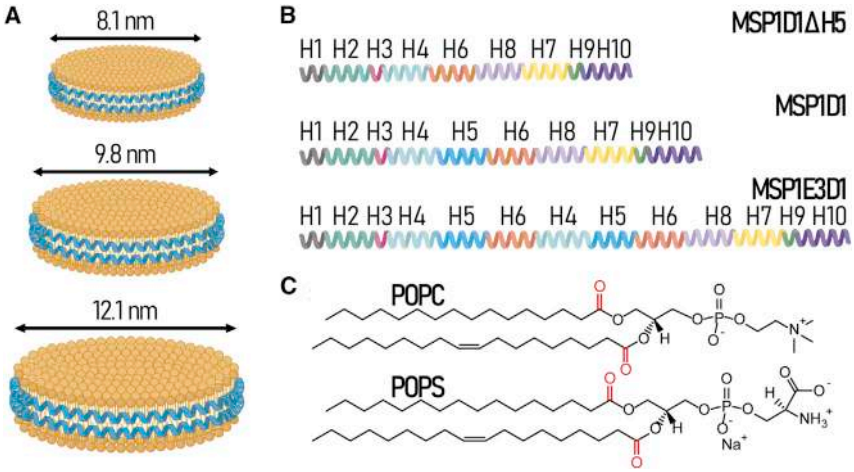

FIGURE 1 (*A*) Illustration of assembled lipid nanodiscs of three sizes employed in this study. The membrane scaffold protein (MSP) is shown as a blue helix. (*B*) Schematics of the MSP variants used to form the corresponding nanodiscs in (*A*); the nomenclature "H1," "H2," etc., describes different α-helical sections of the apolipoprotein A-1 sequence used to engineer distinct MSP variants. (*C*) Chemical structures of the phospholipids used in this study. The ester carbonyls are shown in red.

pump delay time. The pump and probe pulses were maintained at perpendicular polarizations to reduce pump scatter.

RESULTS AND DISCUSSION

Molecular architectures and dimensions of nanodiscs

The most frequently used method for preparing lipid nanodiscs employs an amphipathic protein that encircles a small lipid bilayer, forming a soluble disc-shaped assembly (9,10). MSP is an engineered protein derived from human apolipoprotein A-1, the major protein of high-density lipoprotein particles. The length of the MSP enables precise control over the nanodisc size (Fig. 1 *A*) (9,48). Furthermore, the lipid composition can be adapted to obtain specific protein-membrane interactions, enabling the tuning of lipid headgroup size, polarity, H-bonding ability, and surface charge, which strongly impact interfacial structure and dynamics (41). Phosphatidylcholines are commonly used for nanodisc preparations, but certain proteins require other zwitterionic lipids such as phosphatidylethanolamines or anionic lipids such as phosphatidylserines.

Spectroscopic measurements were carried out for nanodiscs formed from the MSPs shown in Fig. 1 *B* and containing the phospholipids in Fig. 1 *C*. In short, nanodisc assemblies were prepared by using established procedures based on the production and purification of MSP1D1, MSP1D1ΔH5, and MSP1E3D1 proteins mixed with POPC, POPS, or 50:50 molar ratio mixtures of the two lipids, as described in Section S1. The goal of the experimental design was to investigate the H-bond populations and dynamics in nanodiscs made with various MSP and lipid compositions to explore the influence of nanodisc size as well as net charge of the phospholipid headgroups on the extended H-bond network at lipid-water interfaces.

Interfacial H-bond environments in vesicles and nanodiscs

The lipid-water interface produces an H-bond environment markedly different from that of bulk water, stabilizing lipid-lipid interactions and driving the dynamics of both water and lipids (40–44). Lipid ester carbonyl groups (Fig. 1 *C*) serve as internal vibrational reporters of the interfacial environment. The carbonyl stretch absorption band is well represented by two Gaussian peaks centered around 1,730 and 1,745 cm^{-1}, which correspond to the H-bonded (1 H-bond) and free (0 H-bond) carbonyl groups, respectively (Fig. 2) (42).

The absorption spectra of POPC and POPS lipid vesicles and nanodiscs formed from MSP1D1 containing POPC and POPS are shown in Fig. S1 *A*. Spectra

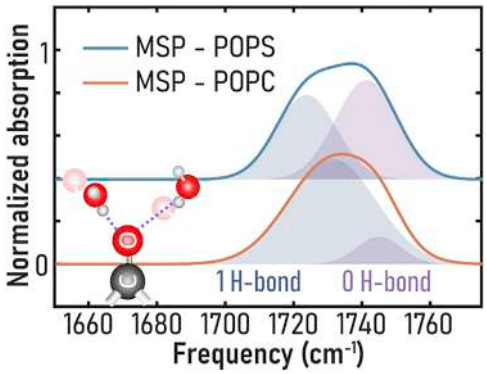

FIGURE 2 IR absorption band of POPC and POPS carbonyl stretching modes with 2-peak gaussian fitting, representing the H-bonded (1,730 cm^{-1}) and non-H-bonded carbonyl (1,745 cm^{-1}) groups, respectively.

of nanodiscs contain an amide I band around 1,650 cm^{-1}, which corresponds to the ester carbonyl stretch of the MSPs and is well separated from the lipid carbonyl band. Fig. S1 *B* shows the peak shape of the carbonyl stretching mode remains unchanged when comparing nanodiscs containing POPC with POPC vesicles. However, lipid nanodiscs with different lipid compositions have significantly different H-bond populations as a result of the headgroup net charge (49). For example, POPC has a significantly higher 1 H-bond population compared with POPS (Fig. 2).

The peak frequency is also correlated with the H-bond strength (50,51). Observing the peak positions of the H-bonded and non-bonded peaks in nanodiscs with lipid vesicles (Fig. 3), we found that the center frequency remained relatively unchanged with composition in vesicles, while there was some variation in the peak positions in the nanodiscs, as observed in the large error bars indicating a broader distribution of environments. These observations are consistent with the simulation studies that show rim lipids carrying different properties than the center lipids (36). A similar trend of increasing frequency of the 1 H-bond peak is observed in both vesicles and nanodiscs.

Enthalpy of H-bonding via temperature-dependent FTIR

H-bond enthalpies can be calculated from temperature-dependent FTIR spectra using a simple van't Hoff analysis, as described previously (44). The measured values in Fig. 3 *B* correspond to the H-bond enthalpies of the lipid carbonyl groups. Because the H-bond enthalpy of a fully water-exposed carbonyl group is 6.6 kJ/mol (52), a higher enthalpy shows that carbonyl groups form a stronger H-bond compared with a similar carbonyl in bulk water. In all samples studied, the H-bond enthalpy is larger than bulk water due to

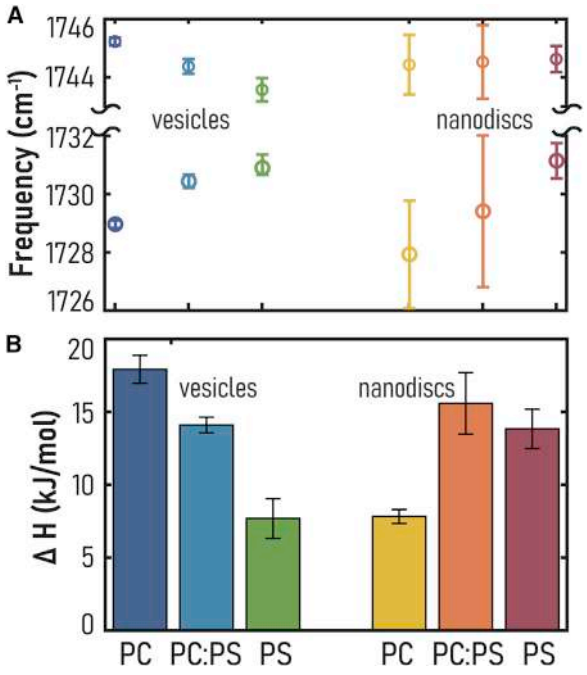

FIGURE 3 (*A*) Experimentally measured FTIR peak positions and (*B*) H-bond enthalpies of vesicles and nanodiscs containing POPC, a 50:50 mixture of POPC, and pure POPS, respectively. All nanodiscs in this dataset were formed with MSP1D1 and have an average diameter of ∼10 nm.

the confined environment of the lipid-water interface. POPC lipids in nanodiscs show significantly reduced H-bond enthalpy compared with POPC in vesicles, and POPS in nanodiscs show increased H-bond enthalpy compared with POPS in vesicles. These differences suggest a role of MSP-lipid interactions that influence H-bond enthalpies. Previous results from molecular dynamics simulations showed highly ordered lipids at the center of the nanodisc and remarkably disordered annular lipids that are in contact with the MSP proteins (36). We conclude that the center and annular lipids have a competing impact on the overall H-bond enthalpy and that this effect is headgroup-charge dependent, suggesting that the lipid ordering and the distribution within the mixed-lipid nanodiscs may not be uniform.

H-bond dynamics measured with 2D IR

Ultrafast 2D IR spectroscopy directly probes local dynamics in heterogeneous systems by measuring the picosecond frequency fluctuations of a vibrational probe (53–55). Here, we studied interfacial H-bond dynamics by using 2D IR to measure the frequency fluctuations of carbonyl probes in lipid nanodiscs and vesicles (Fig. 4). Example 2D IR spectra in Fig. 4 *A* show the ∼1,740 cm^{-1} carbonyl region as well as the 1,640–1,680 cm^{-1} amide I band corresponding to the MSP amide carbonyls, which was not analyzed here. The positive red lobe along the diagonal line and the negative blue lobe correspond to the fundamental ($\nu = 0 \rightarrow 1$) and excited state ($\nu = 1 \rightarrow 2$) transitions, respectively. The correlation between the excitation (pump) and the detection (probe) frequencies results in peak elongation along the diagonal at early waiting times (pump-probe delay, t_2). The peaks become rounder with increasing waiting time; the peak elongation is captured using a center-line-slope analysis as shown in Fig. 4 *B* (56,57). Exponential fitting to the center-line-slope decays in Fig. 4 *C* yielded the relaxation time of the carbonyl frequency-frequency correlation function (58). The fluctuations in frequency are driven by the local H-bond fluctuations, and therefore, the decay timescales are a measure of the local H-bond lifetime.(40,41).

Fig. 4 *D* shows a comparison of H-bond dynamics in nanodiscs and vesicles of the same lipid composition. Overall, nanodiscs exhibit similar dynamics as the vesicles, suggesting that the interfacial water dynamics are largely the same in both systems. However, the dynamics are somewhat affected by lipid composition as well as nanodisc size. In vesicles, we have previously found that the presence of H-bond-donating headgroups leads to faster dynamics due to a combination of interfacial water and lipid-lipid H-bonds (42). Here, the POPC:POPS vesicles experience faster dynamics than POPC vesicles, in agreement with previous observations (42). However, this influence becomes negligible in nanodiscs, as the relaxation time in nanodiscs shows essentially no dependence on the lipid composition. Instead, the effect of nanodiscs sizes on the dynamics are more pronounced, as shorter MSPs result in shorter relaxation times (Fig. 4 *D*). Combined with previous observation of central, boundary, and intermediate lipids from electron paramagnetic resonance spectroscopy and molecular dynamics simulations (59), we conclude that the size dependence is due to the presence of a heterogeneous lipid environment within the nanodiscs, containing both annular lipids adjacent to the MSP and central lipids that do not interact with the MSP. In smaller nanodiscs, the annular lipids make up a larger fraction of the overall lipids. Thus, the observed longer frequency fluctuation relaxation timescales with increasing nanodisc size suggest that the annual lipids may experience faster dynamics, which is consistent with the interpretation that the annular region is more disordered and more solvent exposed. Indeed, increased solvent exposure correlates with faster dynamics (44). However, this effect is relatively minor, and H-bond dynamics can be approximately considered independent of nanodisc size. Thus, the results indicate

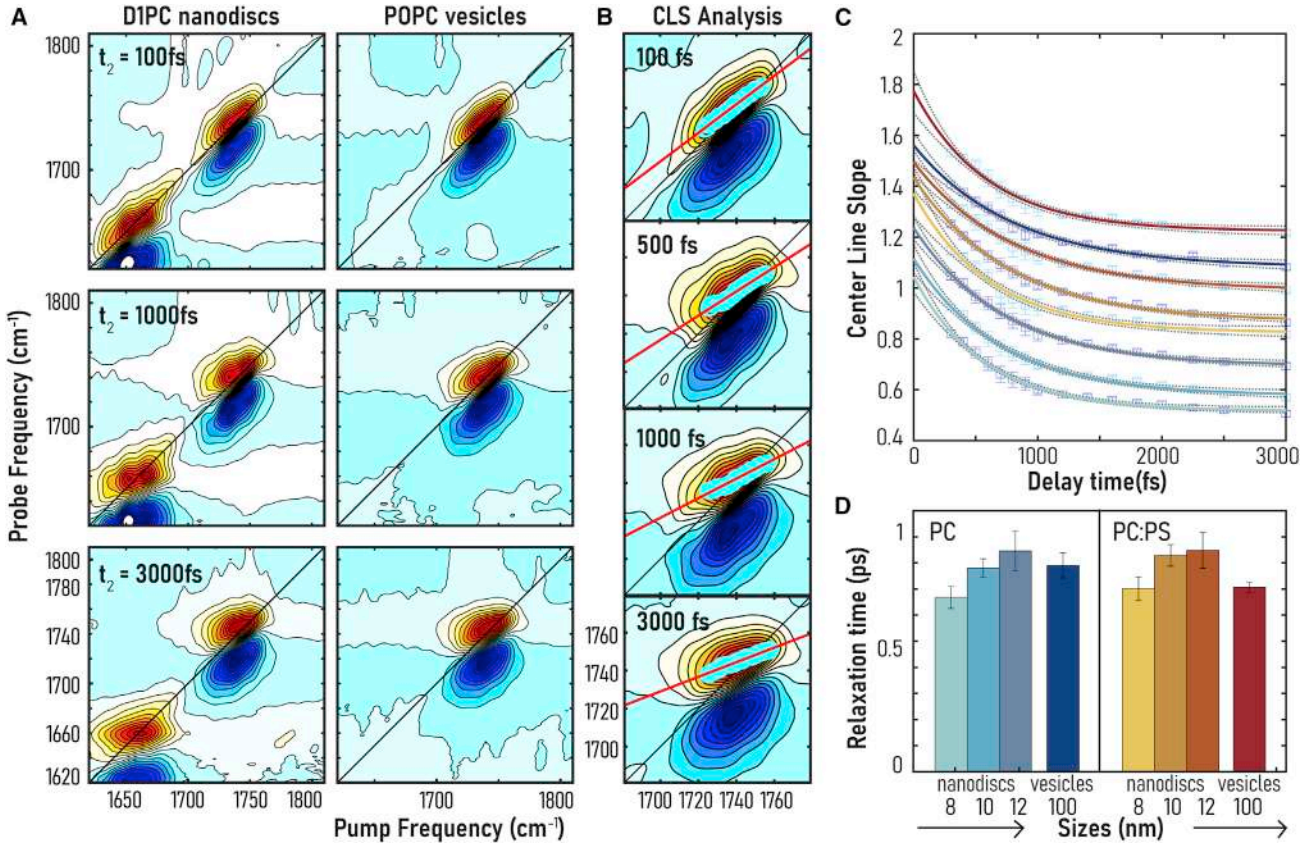

FIGURE 4 (*A*) Representative ester carbonyl 2D IR spectra of nanodiscs and vesicles at short and long waiting times as indicated in the insets. The nanodisc 2D IR shows the amide I band from MSPs (1,650 cm^{-1}) and carbonyl stretching mode from lipids (~1,730–1,745 cm^{-1}). (*B*) Center-line-slope (CLS) analysis of four example 2D IR spectra of POPC vesicles; the slope (red line) decays with waiting time t_2 as the frequency correlation is lost. (*C*) CLS decay curves (squares) with single exponential fitting (solid lines). The fitted curves are vertically offset for display, and the color scheme corresponds to the samples in (*D*). (*D*) Relaxation time constants obtained from single exponential fitting of the CLS curves in (*C*). The sample labeled "PC" represents POPC, and "PC:PS" represents a 1:1 molar ratio mixture of POPC and POPS.

that nanodiscs provide an environment that is largely similar to vesicles, with the caveat that annular lipids are more disordered and solvent exposed.

CONCLUSIONS

We investigated the interfacial environment and ultrafast dynamics of lipids in nanodiscs formed from three MSPs of different lengths and compared the H-bond structure, enthalpy, and dynamics of lipids in nanodiscs with vesicles of the same lipid composition. The main finding is the overall lipid-water interfaces in nanodiscs are largely similar to those in lipid vesicles. However, the two environments are not identical, and our data suggest MSPs perturb annular lipids within nanodiscs, as evidenced by higher heterogeneity of the H-bond environment. In nanodiscs, the influence of lipid headgroup net charge on H-bond dynamics is diminished, potentially due to MSP-lipid interactions. In contrast to lipid vesicles, the H-bond-donating capacity does not have a substantial effect on H-bond dynamics in nanodiscs. The interfacial H-bond dynamics are faster in the smallest nanodiscs compared with the largest nanodiscs, likely because the proportion of annular lipids is larger in smaller nanodiscs. These results indicate that nanodisc size may be an important consideration when choosing which nanodisc system to use for membrane protein studies. Considering that the insertion of large membrane proteins further changes the center-to-rim ratio of lipids, a larger lipid nanodisc system should more closely resemble the lipid vesicles. Overall, however, we observe that nanodiscs provide an interfacial environment that is similar to vesicles with only minor differences noted above, and thus nanodiscs are reasonably suitable membrane mimetics for protein studies.

SUPPORTING MATERIAL

Supporting material can be found online at https://doi.org/10.1016/j.bpr.2022.100066.

AUTHOR CONTRIBUTIONS

X.Y., N.T., A.P.R. prepared samples, performed research, analyzed data, and wrote the manuscript. M.T.E. and C.R.B. designed and supervised the research and wrote the manuscript.

ACKNOWLEDGMENTS

M.T.E., N.T., and A.P.R. were supported by the National Institutes of Health MIRA grant (R35GM138291). C.R.B. and X.Y. were supported by the National Institutes of Health (R35GM133359), as well as through a grant from the Welch Foundation (F-1891).

DECLARATION OF INTERESTS

The authors declare no competing interests.

REFERENCES

1. Yeagle, P. L. 2016. Chapter 10 - membrane proteins. *In* The Membranes of Cells, Third edition. P. L. Yeagle, ed. Academic Press, pp. 219–268.
2. Escribá, P. V., J. M. González-Ros, …, G. Barceló-Coblijn. 2008. Membranes: a meeting point for lipids, proteins and therapies. *J. Cell Mol. Med.* 12:829–875.
3. Bogdanov, M., W. Dowhan, and H. Vitrac. 2014. Lipids and topological rules governing membrane protein assembly. *Biochim. Biophys. Acta.* 1843:1475–1488.
4. Gustot, A., J.-M. Ruysschaert, …, C. Govaerts. 2010. Lipid composition regulates the orientation of transmembrane helices in HorA, an ABC multidrug transporter. *J. Biol. Chem.* 285:14144–14151.
5. Cymer, F., A. Veerappan, and D. Schneider. 2012. Transmembrane helix–helix interactions are modulated by the sequence context and by lipid bilayer properties. *Biochim. Biophys. Acta.* 1818:963–973.
6. Lee, A. G. 2003. Lipid-protein interactions in biological membranes: a structural perspective. *Biochim. Biophys. Acta.* 1612:1–40.
7. Lee, A. G. 2004. How lipids affect the activities of integral membrane proteins. *Biochim. Biophys. Acta.* 1666:62–87.
8. Phillips, R., T. Ursell, …, P. Sens. 2009. Emerging roles for lipids in shaping membrane-protein function. *Nature.* 459:379–385.
9. Denisov, I. G., Y. V. Grinkova, …, S. G. Sligar. 2004. Directed self-assembly of monodisperse phospholipid bilayer Nanodiscs with controlled size. *J. Am. Chem. Soc.* 126:3477–3487.
10. Bayburt, T. H., Y. V. Grinkova, and S. G. Sligar. 2002. Self-Assembly of Discoidal Phospholipid Bilayer Nanoparticles with Membrane Scaffold Proteins. *Nano Lett.* 2:853–856.
11. Hagn, F., M. L. Nasr, and G. Wagner. 2018. Assembly of phospholipid nanodiscs of controlled size for structural studies of membrane proteins by NMR. *Nat. Protoc.* 13:79–98.
12. Raschle, T., S. Hiller, …, G. Wagner. 2009. Structural and functional characterization of the integral membrane protein VDAC-1 in lipid bilayer nanodiscs. *J. Am. Chem. Soc.* 131:17777–17779.
13. Sušac, L., R. Horst, and K. Wüthrich. 2014. Solution-NMR characterization of outer-membrane protein A from E. coli in lipid bilayer nanodiscs and detergent micelles. *Chembiochem.* 15:995–1000.
14. Li, Y., A. Z. Kijac, …, C. M. Rienstra. 2006. Structural analysis of nanoscale self-assembled discoidal lipid bilayers by solid-state NMR spectroscopy. *Biophys. J.* 91:3819–3828.
15. Lakomek, N. A., L. Frey, …, B. H. Meier. 2017. Proton-Detected NMR Spectroscopy of Nanodisc-Embedded Membrane Proteins: MAS Solid-State vs Solution-State Methods. *J. Phys. Chem. B.* 121:7671–7680.
16. Frey, L., N. A. Lakomek, …, S. Bibow. 2017. Micelles, Bicelles, and Nanodiscs: Comparing the Impact of Membrane Mimetics on Membrane Protein Backbone Dynamics. *Angew. Chem. Int. Ed. Engl.* 56:380–383.
17. Günsel, U., and F. Hagn. 2021. Lipid nanodiscs for high-resolution NMR studies of membrane proteins. *Chem. Rev.* 122:9395–9421.
18. Wei, S., N. Thakur, …, R. Lamichhane. 2022. Slow conformational dynamics of the human A2A adenosine receptor are temporally ordered. *Structure.* 30:329–337.e5.
19. Nath, A., A. J. Trexler, …, E. Rhoades. 2010. Single-molecule fluorescence spectroscopy using phospholipid bilayer nanodiscs. *In* Methods in Enzymology. Elsevier, pp. 89–117.
20. Nath, A., P. K. Koo, …, W. M. Atkins. 2008. Allosteric effects on substrate dissociation from cytochrome P450 3A4 in nanodiscs observed by ensemble and single-molecule fluorescence spectroscopy. *J. Am. Chem. Soc.* 130:15746–15747.
21. Lamichhane, R., J. J. Liu, …, D. P. Millar. 2015. Single-molecule view of basal activity and activation mechanisms of the G protein-coupled receptor beta2AR. *Proc. Natl. Acad. Sci. USA.* 112:14254–14259.
22. Zhang, M., M. Gui, …, G. Wagner. 2021. Cryo-EM structure of an activated GPCR-G protein complex in lipid nanodiscs. *Nat. Struct. Mol. Biol.* 28:258–267.
23. Matthies, D., C. Bae, …, K. J. Swartz. 2018. Single-particle cryo-EM structure of a voltage-activated potassium channel in lipid nanodiscs. *Elife.* 7:e37558.
24. Kern, D. M., B. Sorum, …, S. G. Brohawn. 2021. Cryo-EM structure of SARS-CoV-2 ORF3a in lipid nanodiscs. *Nat. Struct. Mol. Biol.* 28:573–582.
25. Kalienkova, V., C. Alvadia, …, C. Paulino. 2020. Single-Particle Cryo-EM of Membrane Proteins. *In* Lipid Nanodiscs. Expression, Purification, and Structural Biology of Membrane Proteins. C. Perez and T. Maier, eds. Springer US, pp. 245–273.
26. Redhair, M., A. F. Clouser, and W. M. Atkins. 2019. Hydrogen-deuterium exchange mass spectrometry of membrane proteins in lipid nanodiscs. *Chem. Phys. Lipids.* 220:14–22.
27. Kostelic, M. M., C. K. Zak, …, M. T. Marty. 2021. Assembly of model membrane nanodiscs for native mass spectrometry. *Anal. Chem.* 93:5972–5979.
28. Walker, L. R., E. M. Marzluff, …, M. T. Marty. 2019. Native mass spectrometry of antimicrobial peptides in lipid nanodiscs elucidates complex assembly. *Anal. Chem.* 91:9284–9291.
29. Denisov, I. G., and S. G. Sligar. 2017. Nanodiscs in membrane biochemistry and biophysics. *Chem. Rev.* 117:4669–4713.
30. Denisov, I. G., and S. G. Sligar. 2016. Nanodiscs for structural and functional studies of membrane proteins. *Nat. Struct. Mol. Biol.* 23:481–486.
31. Brown, C. J., C. Trieber, and M. Overduin. 2021. Structural biology of endogenous membrane protein assemblies in native nanodiscs. *Curr. Opin. Struct. Biol.* 69:70–77.
32. Majeed, S., A. B. Ahmad, …, E. R. Georgieva. 2021. Lipid Membrane mimetics in functional and structural studies of integral membrane proteins. *Membranes.* 11:685.
33. Debnath, A., and L. V. Schäfer. 2015. Structure and dynamics of phospholipid nanodiscs from all-atom and coarse-grained simulations. *J. Phys. Chem. B.* 119:6991–7002.
34. Shih, A. Y., I. G. Denisov, …, K. Schulten. 2005. Molecular dynamics simulations of discoidal bilayers assembled from truncated human lipoproteins. *Biophys. J.* 88:548–556.
35. Siuda, I., and D. P. Tieleman. 2015. Molecular Models of Nanodiscs. *J. Chem. Theor. Comput.* 11:4923–4932.

36. Bengtsen, T., V. L. Holm, …, K. Lindorff-Larsen. 2020. Structure and dynamics of a nanodisc by integrating NMR, SAXS and SANS experiments with molecular dynamics simulations. *Elife.* 9:e56518.
37. Martinez, D., M. Decossas, …, A. Loquet. 2017. Lipid internal dynamics probed in nanodiscs. *ChemPhysChem.* 18:2651–2657.
38. Skar-Gislinge, N., J. B. Simonsen, …, L. Arleth. 2010. Elliptical structure of phospholipid bilayer nanodiscs encapsulated by scaffold proteins: casting the roles of the lipids and the protein. *J. Am. Chem. Soc.* 132:13713–13722.
39. Boettcher, J. M., R. L. Davis-Harrison, …, C. M. Rienstra. 2011. Atomic View of Calcium-Induced Clustering of Phosphatidylserine in Mixed Lipid Bilayers. *Biochemistry.* 50:2264–2273.
40. Flanagan, J. C., A. E. Cardenas, and C. R. Baiz. 2020. Ultrafast spectroscopy of lipid-water interfaces: transmembrane crowding drives H-bond dynamics. *J. Phys. Chem. Lett.* 11:4093–4098.
41. Flanagan, J. C., M. L. Valentine, and C. R. Baiz. 2020. Ultrafast dynamics at lipid-water interfaces. *Acc. Chem. Res.* 53:1860–1868.
42. Valentine, M. L., M. K. Waterland, …, C. R. Baiz. 2021. Interfacial dynamics in lipid membranes: the effects of headgroup structures. *J. Phys. Chem. B.* 125:1343–1350.
43. Venkatraman, R. K., and C. R. Baiz. 2020. Ultrafast dynamics at the lipid-water interface: DMSO modulates H-bond lifetimes. *Langmuir.* 36:6502–6511.
44. You, X., E. Lee, …, C. R. Baiz. 2021. Molecular mechanism of cell membrane protection by sugars: a study of interfacial H-bond networks. *J. Phys. Chem. Lett.* 12:9602–9607.
45. Baiz, C. R., B. Błasiak, …, M. T. Zanni. 2020. Vibrational spectroscopic map, vibrational spectroscopy, and intermolecular interaction. *Chem. Rev.* 120:7152–7218.
46. Bayburt, T. H., and S. G. Sligar. 2010. Membrane protein assembly into nanodiscs. *FEBS Lett.* 584:1721–1727.
47. Edington, S. C., A. Gonzalez, …, C. R. Baiz. 2018. Coordination to lanthanide ions distorts binding site conformation in calmodulin. *Proc. Natl. Acad. Sci. USA.* 115:E3126–E3134. https://doi.org/10.1073/pnas.1722042115.
48. Hagn, F., M. Etzkorn, …, G. Wagner. 2013. Optimized phospholipid bilayer nanodiscs facilitate high-resolution structure determination of membrane proteins. *J. Am. Chem. Soc.* 135:1919–1925.
49. Valentine, M. L., A. E. Cardenas, …, C. R. Baiz. 2018. Physiological calcium concentrations slow dynamics at the lipid-water interface. *Biophys. J.* 115:1541–1551.
50. DeCamp, M. F., L. DeFlores, …, M. Cho. 2005. Amide I vibrational dynamics of N-methylacetamide in polar solvents: the role of electrostatic interactions. *J. Phys. Chem. B.* 109:11016–11026.
51. Ham, S., S. Cha, …, M. Cho. 2003. Amide I modes of tripeptides: Hessian matrix reconstruction and isotope effects. *J. Chem. Phys.* 119:1451–1461.
52. Guerin, A. C., K. Riley, …, D. G. Kuroda. 2016. Determining the energetics of the hydrogen bond through FTIR: a hands-on physical chemistry lab experiment. *J. Chem. Educ.* 93:1124–1129.
53. Hamm, P., and M. Zanni. 2011. Concepts and Methods of 2D Infrared Spectroscopy. Cambridge University Press.
54. Zheng, J., K. Kwak, and M. D. Fayer. 2007. Ultrafast 2D IR vibrational echo spectroscopy. *Acc. Chem. Res.* 40:75–83.
55. Khalil, M., N. Demirdöven, and A. Tokmakoff. 2003. Coherent 2D IR spectroscopy: molecular structure and dynamics in solution. *J. Phys. Chem. A.* 107:5258–5279.
56. Guo, Q., P. Pagano, …, C. M. Cheatum. 2015. Line shape analysis of two-dimensional infrared spectra. *J. Chem. Phys.* 142:212427.
57. Kwak, K., S. Park, …, M. D. Fayer. 2007. Frequency-frequency correlation functions and apodization in two-dimensional infrared vibrational echo spectroscopy: A new approach. *J. Chem. Phys.* 127:124503.
58. Kwak, K., D. E. Rosenfeld, and M. D. Fayer. 2008. Taking apart the two-dimensional infrared vibrational echo spectra: More information and elimination of distortions. *J. Chem. Phys.* 128:204505.
59. Stepien, P., B. Augustyn, …, T. Rog. 2020. Complexity of seemingly simple lipid nanodiscs. *Biochim. Biophys. Acta Biomembr.* 1862:183420.